DOI:10.1190/image2022-3751372.1

Elastic FWI application to a land data set in the Middle East

Anna Sedova, Olivier Leblanc, Thibaut Allemand, Gilles Lambaré, Stéphane Pellerin, Daniela Donno, CGG*

Summary

Seismic imaging is particularly challenging in the Middle East. The shallow geology is often characterized by strong velocity contrasts from layered sands and carbonates that create multiples and mode conversions. Capturing these velocity variations is essential for accurate imaging. While recent developments in full-waveform inversion (FWI) make it a powerful velocity model building tool, its application to land data, with poorer data quality and stronger elastic effects, remains challenging. Elastic FWI further advances velocity model building in these complex geological settings, allowing for a more physically accurate description of the subsurface. We present a workflow based on a combination of diving-wave anisotropic elastic FWI and joint refraction-reflection tomography. With synthetic and real data, we show that it permits inverting a larger part of the diving-wave train compared to acoustic FWI. With the real data example, we demonstrate the Vp model inverted from elastic FWI gives better focused stack image with improved event continuity and flatter gathers with enhanced coherence.

Introduction

The geological structure of the Middle East is often characterized by strong velocity contrasts in the top kilometer of the subsurface due to layered sand and carbonate formations (Bharti et al., 2016). The associated strong internal multiples (El-Emam et al., 2012) and mode conversions are particularly challenging for velocity model building and imaging. Characterizing this part of the velocity model is necessary for accurate imaging of deeper structures. Reflection-based tomography is penalized by the low fold of the data, low signal-to-noise ratio (S/N), and multiples. It can be combined with refraction tomography, surface-wave inversion, or other multi-physics techniques (Bardainne, 2018; Speziali et al., 2019; Rebert et al., 2022), but the development of land FWI offers promising new opportunities.

Several successful examples of land FWI applications in the Middle East have been published (Stopin et al., 2014; Cheng et al., 2017; Sedova et al., 2019; Hermant et al., 2020; Masclet et al., 2021). It has also been observed that the acoustic approximation could suffer in geologically complex areas with high velocity contrasts (Plessix and Pérez Solano, 2015; Pérez Solano and Plessix, 2019). A solution to mitigate the impact of elastic effects when applying diving-wave acoustic land FWI is to limit the data mute to very early arrivals (Cheng et al., 2017). However, Stopin et al. (2014) and Cheng et al. (2017) also report that artifacts start to appear when increasing frequencies above 8 Hz and mention that it could be caused by elastic effects. This motivated elastic FWI investigations to solve the challenges of land FWI in the Middle East (Plessix and Pérez Solano, 2015; Bharti et al., 2016; Pérez Solano and Plessix, 2019; Adwani et al., 2021).

We present an elastic land FWI workflow for anisotropic velocity model building. The workflow leans both on an elastic land FWI algorithm (Leblanc et al., 2022) and the acoustic land FWI experience based on diving-wave inversion (Sedova et al., 2019; Messud et al., 2021), combined with joint refraction-reflection tomography (Allemand et al., 2020). One key difference between the applications of elastic and acoustic FWI on land data is the portion of the data that is used to generate model updates. To illustrate this point, we present synthetic tests that analyze the influence of data selection on the inversion results. We then apply the same data selection strategy to a real land data example. For our tests, we employ the 3D VTI elastic land FWI algorithm presented by Leblanc et al. (2022).

Elastic land FWI

There are specific challenges to elastic land FWI. One of the key points is the selection of the data entering the inversion. Aiming to invert the diving waves and faced with the challenge of low-frequency ground-roll removal, Plessix and Pérez Solano (2015) propose a modified boundary condition used in several elastic land FWI applications in the Middle East (Bharti et al., 2016; Pérez Solano and Plessix, 2019). Going a step further, He et al. (2019) and Adwani et al. (2020) propose to jointly invert diving and surface waves (using a free-surface condition), emphasizing their complementary role in retrieving elastic Earth parameters.

In line with these conclusions, Leblanc et al. (2022) stress the importance of using a free-surface condition rather than a modified boundary condition. Indeed, when inverting diving waves with long-offset data, the mute of the ground roll can be easily determined, while the use of a modified boundary condition significantly reduces the part of the diving-wave train that can be accurately interpreted. Therefore, we consider diving-wave elastic land FWI with a free-surface condition.

Elastic versus acoustic diving-wave land FWI

It is critical to evaluate the update in quality of elastic land FWI in the Middle East compared to the computationally less intensive acoustic land FWI. With this objective in mind, we first perform a synthetic modeling exercise. We design an isotropic elastic velocity model derived from a well log, shown in Figure 5, that exhibits important shallow velocity contrasts typical of the challenging Middle East geology. V_P is a smoothed version of the log and V_S is derived from a constant V_P/V_S ratio inferred from regional knowledge.

By overlaying the resulting acoustic and elastic data modeled at 5 Hz (Figure 1), we observe that both data sets are

similar at early arrivals but exhibit significant differences at later arrivals due to elastic mode conversions. This exercise indicates that acoustic FWI may require a more severe inner mute (yellow line in Figure 1) to isolate usable data to properly converge, as illustrated by Cheng et al. (2017). The mute is critical to avoid most of the phase differences caused by elastic effects.

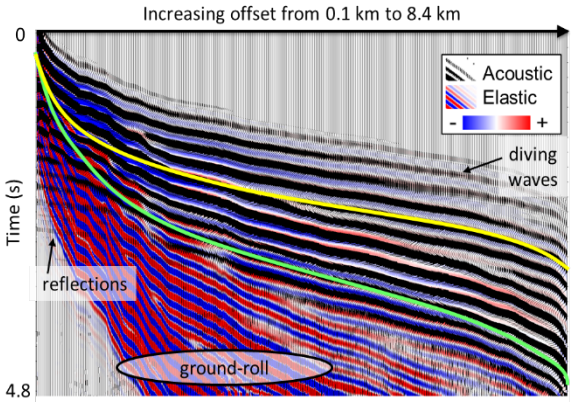

Figure 1: Modeled acoustic data in wiggle overlaid on top of modeled elastic data in blue-white-red. Several shot lines are displayed, and traces are sorted by increasing offset. The inner mutes used for the acoustic and elastic FWI are indicated by the yellow and green lines, respectively.

To further analyze the impact of the acoustic approximation on the inversion results, we generate another synthetic laterally invariant velocity model, again inspired by the geology of the Middle East. Figures 2e and 2f show the V_P model as a black curve. V_S is derived from a constant V_P/V_S ratio and density is constant. We compute an elastic synthetic seismogram with 12 km maximum offset. The source signature frequency band ranges from 1.5 to 12 Hz. Starting from an erroneous smoothed version of the true velocity (yellow line in Figures 2e and 2f), we perform acoustic and elastic FWI from 2 to 12 Hz. An Optimal Transport FWI objective function (Messud et al., 2021) is used for the initial low frequencies, and a least-squares objective function is used for higher frequencies.

Figure 2 shows the resulting V_P velocity models and the associated data QC for acoustic and elastic FWI. While the elastic FWI converges towards the true model (red line in Figure 2e and 2f), the acoustic FWI does not converge when using the same inner mute (blue line in Figure 2e). The data fit when using acoustic FWI (Figure 2c) is compared to elastic FWI (Figure 2b).

A more severe inner mute allows acoustic FWI to recover the long wavelengths of the velocity model (blue line in Figure 2f). However, it struggles to retrieve the first velocity inversion at approximately 400 m, due to the limited portion of the diving-wave train that it can interpret (Figure 2d).

Our analysis shows that elastic FWI enables the interpretation of a larger portion of seismic data, which increases the vertical resolution of the resulting shallow velocity model. For real data application, the inner mute for elastic and acoustic FWI can be chosen based on analysis of the observed data and a modeling exercise similar to the one shown in Figure 1.

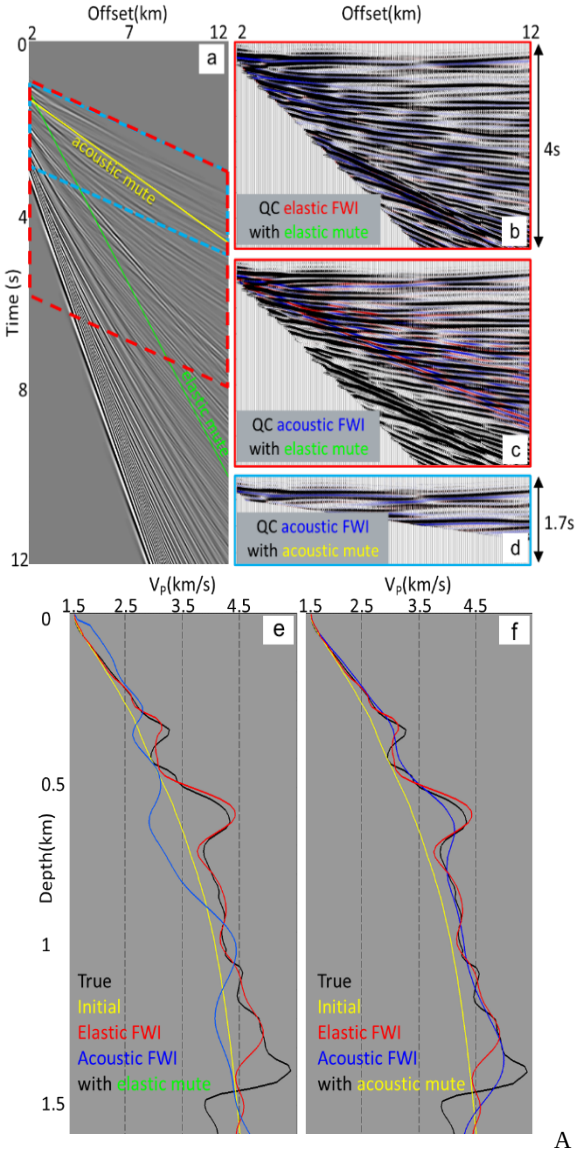

A

Figure 2: Synthetic case: a) observed data, mutes, and location of red and blue boxes for QCs shown in b, c, d. b, c, and d) data fit QC: observed (wiggle) versus modeled data (blue/red) for the final 12 Hz elastic FWI model (b), and acoustic FWI models obtained with elastic (c) and acoustic mutes (d). e and f) V_P profiles: true model (black line), initial model (yellow line) and models inverted with elastic FWI (red line) and acoustic FWI (blue lines), with elastic (e) and acoustic (f) mutes.

Elastic FWI application to a land data set in the Middle East

Application to real data

We applied our elastic land FWI to a 231 km^2 subset of a 2012 acquisition in the Middle East. The survey was acquired using vibroseis sources with a sweep of 2 to 84 Hz. The maximum offset used for the test is 9 km.

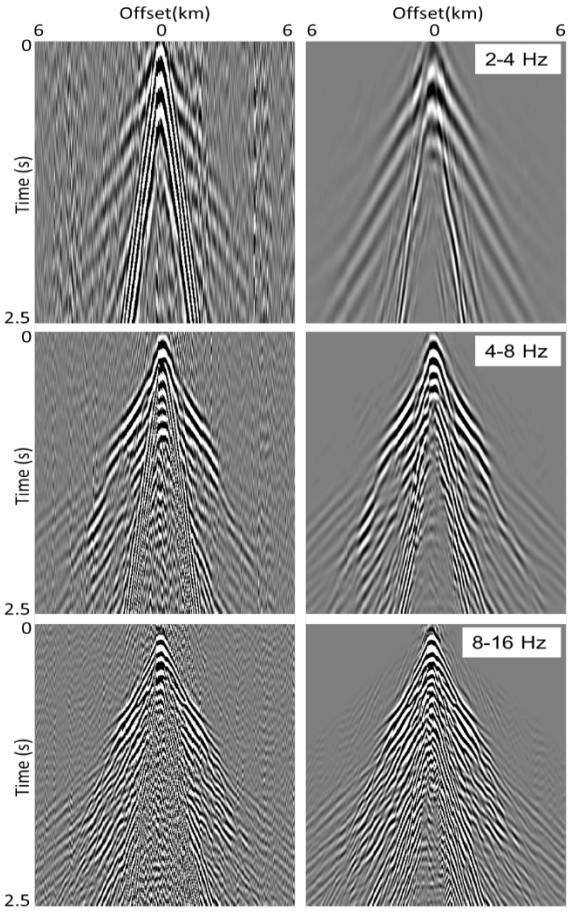

Figure 3: Dedicated pre-processing per octave: left) raw data after despiking, and right) after all pre-processing steps.

We focus on the inversion of diving waves. Their pre-processing (Figure 3) aims to improve the S/N at low frequencies and long offsets. It includes de-spiking, 3D ground roll attenuation, and random noise attenuation (Sedova et al., 2019). As shown in Figure 3, we remove most of the ground-roll energy without damaging the data, and any remaining ground-roll energy may be removed using an inner mute.

The initial V_P (Figure 4a) and V_S models for elastic FWI are derived from the smoothed vintage model and from regional well knowledge, respectively, and combined with the result of multi-wave inversion in the shallow part (Rebert et al., 2022). The diving waves are inverted using the inner mute displayed in Figure 6. Bharti et al. (2016) point out the importance of including anisotropy parameters in FWI. However, we believe that diving-wave FWI struggles to update the long wavelengths of both velocity and anisotropy, due to crosstalk. We therefore use the anisotropic FWI workflow proposed by Allemand et al. (2020). It combines elastic FWI and joint refraction-reflection tomography, allowing to reconcile the kinematics of diving and reflection waves. Two passes of elastic FWI are required. The first one allows to model the first breaks used in joint tomography. The second one uses the resulting vertical transverse isotropic (VTI) ε parameter from the joint tomography.

The V_P velocity model obtained by elastic VTI FWI is displayed in Figure 4b. The velocity inversions (pointed by arrows) corresponding to two important regional geological formations and visible on the sonic log (Figure 5c or 5f) are recovered.

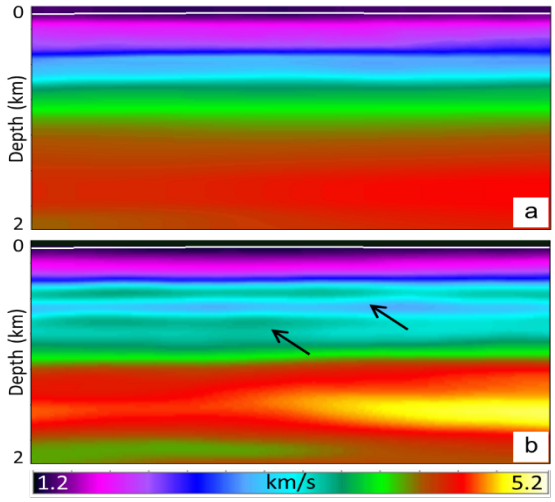

Figure 4: Initial Vp (a) and inverted Vp (b) velocity models obtained by 8 Hz elastic FWI.

Figure 5 displays the migrated stack produced with the final elastic FWI V_P model and the associated common image gathers (CIGs). They are compared with the stack and gathers migrated with the initial V_P model. The velocity model provided by elastic FWI results in a better focused stack image with improved event continuity and flatter gathers with enhanced coherence in the middle part of the section, which contains strong velocity inversions.

Figure 6 (left) shows the good data fit obtained at 8 Hz with the final elastic FWI model, which explains a large part of the selected diving-wave data. For reference, we also perform a similar anisotropic workflow using acoustic FWI, but with a tighter mute (yellow line in Figure 6, right) designed to mitigate the impact of elastic converted events as shown in our synthetic tests. Figure 6 (right) displays the data fit between the same observed data and 8 Hz acoustic modeled data with acoustic FWI inverted model. Although the fit is equally good for acoustic and elastic inversions on the early

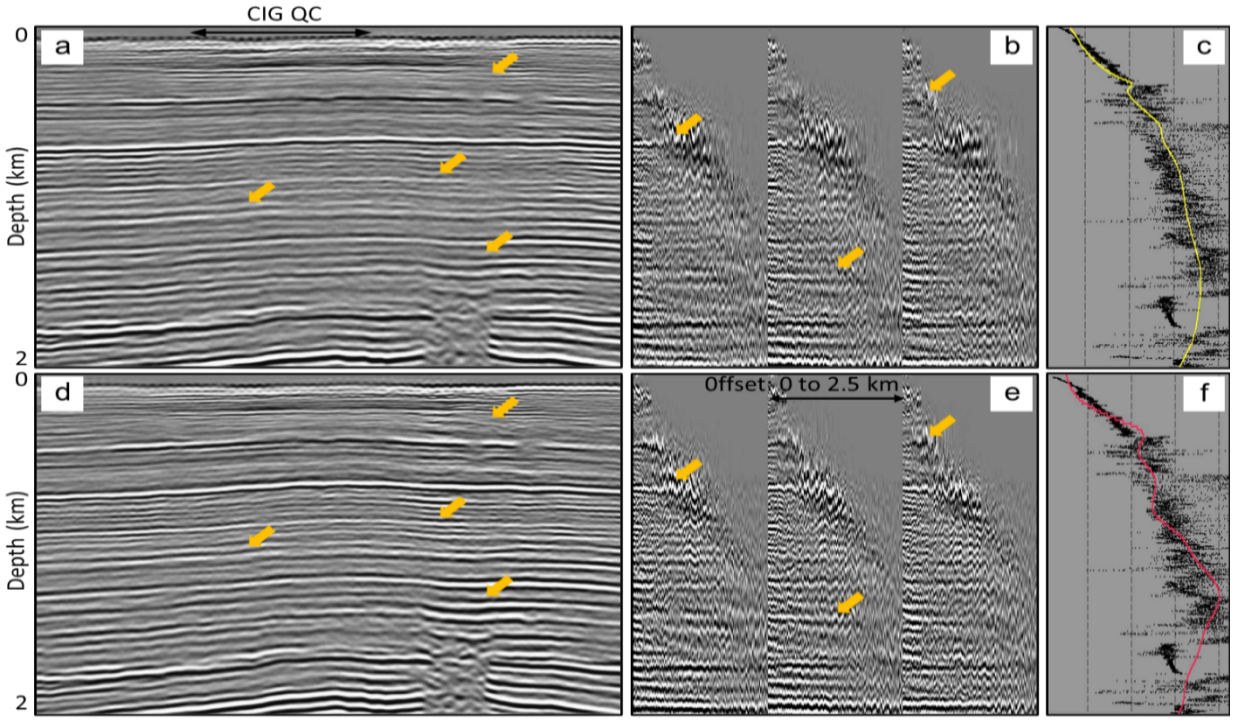

Figure 5: a) Migrated stack with initial velocity model; b) corresponding common image gathers (CIGs); c) initial velocity Vp (yellow curve) over the sonic data (black). d) Migrated stack with the velocity model from elastic FWI workflow; e) corresponding CIGs; f) Vp velocity model updated by elastic FWI (red curve) over the sonic data (black).

events, later events that are related to converted waves could not be interpreted correctly by acoustic FWI. As a result, elastic FWI allows us to use a larger part of the data to obtain a better constrained velocity model for depth imaging, as indicated in the synthetic result of Figure 2.

Conclusions

We describe an anisotropic diving-wave elastic land FWI workflow able to address some challenges of land FWI in the Middle East. We highlight the importance of the mute definition by comparing results obtained from acoustic and elastic FWI. While it is possible to obtain good results with an acoustic approximation using a severe mute (Sedova et al., 2019; Farooqui et al., 2021), the elastic full-wave modeling explains a much larger part of the diving-wave data, resulting in an improved inverted V_P model. An improved near-surface initial model for both V_P and V_S, possibly through FWI of surface waves, could pave the way for joint inversion of diving and surface waves.

Acknowledgments

We thank CGG for permission to present this work and KOC for permission to use the data. We thank Gillian Royle, Chu-Ong Ting, Yi Xie, Nabil Masmoudi, Ping Wang, and other colleagues for constructive remarks.

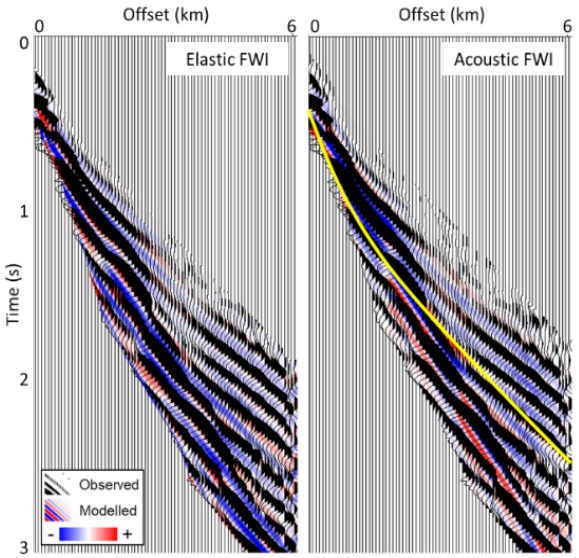

Figure 6: Overlay of observed (wiggle) and modeled data (blue-white-red) obtained with elastic FWI (left) and an equivalent acoustic FWI (right) with a tighter mute (yellow line).

References

Adwani, A., M. Danilouchkine, R. Plessix, A. Soni, M. Jahdhami, S. Abri, F. Ernst, and F. Ten Kroode, 2021, Subsurface imaging with elastic FWI using surface and diving waves: 3D land data from South Oman: 82nd Conference and Exhibition, EAGE, Extended Abstracts, doi: https://doi.org/10.3997/2214-4609.202011345.

Allemand, T., A. Sedova, G. Lambaré, D. Grenié, and P. Guillaume, 2020, Full waveform inversion in an anisotropic earth: A practical workflow: Annual Conference & Exhibition Online, EAGE, Extended Abstracts, doi: https://doi.org/10.3997/2214-4609.202011685.

Bardainne, T., 2018, Joint inversion of refracted P-waves, surface waves and reflectivity: 80th Conference & Exhibition, EAGE, Extended Abstracts, We K 02, doi: https://doi.org/10.3997/2214-4609.201801158.

Bharti, S., A. Stopin, C. A. Pérez Solano, R.-E. Plessix, J. Lutz, B. Al-Qadeeri, Q. Dashti, S. Narhari, and O. O. Kolawole, 2016, Application of an anisotropic elastic multiparameter waveform inversion on a land data set from north Kuwait: 86th Annual International Meeting, SEG, Expanded Abstracts, 1201–1205, doi: https://doi.org/10.1190/segam2016-13862096.1.

Cheng, X., K. Jiao, D. Sun, Z. Xu, D. Vigh, and A. El-Emam, 2017, High-resolution Radon preconditioning for full- waveform inversion of land data: Interpretation, **5**, no. 4, SR23–SR33, doi: https://doi.org/10.1190/INT-2017-0020.1.

El-Emam, A., K. S. Al-Deen, A. Zarkhidze, and A. Walz, 2012, Advances in interbed multiples prediction and attenuation: Case study from onshore Kuwait: 82nd Annual International Meeting, SEG, Expanded Abstracts, 3546–3550, doi: https://doi.org/10.1190/1.3627936.

Farooqui, M. S., D. Carotti, and M. Al-Jahdhami, 2021, Integrated high-resolution model building: A case study from the Sultanate of Oman: 82nd Conference & Exhibition, EAGE, Extended Abstracts, doi: https://doi.org/10.3997/2214-4609.202112701.

He, W., R. Brossier, L. Métivier, and R. E. Plessix, 2019, Land seismic multi-parameter FWI in elastic VTI media by simultaneously interpreting body waves and surface waves: 81st Conference & Exhibition, EAGE, Extended Abstracts, Tu R08 09, doi: https://doi.org/10.3997/2214-4609.201900876.

Hermant, O., A. Aziz, S. Warzocha, and M. Al Jahdhami, 2020, Imaging complex fault structures on-shore Oman using optimal transport full waveform inversion: Annual Conference & Exhibition Online, EAGE, Extended Abstracts, doi: https://doi.org/10.3997/2214-4609.202010734.

Leblanc, O., A. Sedova, G. Lambaré, T. Allemand, O. Hermant, D. Carotti, D. Donno, and N. Masmoudi, 2022, Elastic land full-waveform inversion in the Middle East: Method and applications: 83rd Conference & Exhibition, EAGE, Extended Abstracts, doi: https://doi.org/10.3997/2214-4609.202210375.

Masclet, S., G. Bouquard, and H. Prigent, 2021, Multi-wave and full-waveform inversion in Southern Oman: 82nd Conference & Exhibition, EAGE, Extended Abstracts, doi: https://doi.org/10.3997/2214-4609.202010731.

Messud, J., D. Carotti, O. Hermant, A. Sedova, and G. Lambaré, 2021, Optimal transport full-waveform inversion: From theory to industrial applications with examples from the Sultanate of Oman: First Break, **39**, no. 12, 45–53, doi: https://doi.org/10.3997/1365-2397.fb2021090.

Pérez Solano, C. A., and R.-E. Plessix, 2019, Velocity-model building with enhanced shallow resolution using elastic waveform inversion — An example from onshore Oman: Geophysics, **84**, no. 6, R977–R988, doi: https://doi.org/10.1190/geo2018-0736.1.

Plessix, R.-E., and C. A. Pérez Solano, 2015, Modified surface boundary conditions for elastic waveform inversion of low-frequency wide-angle active land seismic data: Geophysical Journal International, **201**, no. 3, 1324–1334, doi: https://doi.org/10.1093/gji/ggv087.

Rebert, T., L. Vivin, O. Bouhdiche, M. Retailleau, D. Le Meur, A. El-Emam, M. Ali, and H. Bayri, 2022, Depth imaging in North Kuwait: Challenges and solutions: 83rd Conference & Exhibition, EAGE, Extended Abstracts, doi: https://doi.org/10.3997/2214-4609.202210411.

Sedova, A., G. Royle, T. Allemand, G. Lambaré, and O. Hermant, 2019, High-frequency acoustic land full-waveform inversion: A case study from the Sultanate of Oman: First Break, **37**, no. 1, 75–81, doi: https://doi.org/10.3997/1365-2397.n0010.

Speziali, M., A. El-Emam, F. Miotti, M. Mantovani, and A. Mohamed, 2019, Sequential and simultaneous joint inversion: The multiphysics approach to Middle East imaging challenges: 81st Conference and Exhibition, EAGE, Extended Abstracts, Tu R16 14, doi: https://doi.org/10.3997/2214-4609.201900977.

Stopin, A., R.-E. Plessix, and S. Al Abri, 2014, Multiparameter waveform inversion of a large wide azimuth low-frequency land data set in Oman: Geophysics, **79**, no. 3, WA67–WA77, doi: https://doi.org/10.1190/geo2013-0323.1.